LANGMUIR



pubs.acs.org/Langmuir
Article

# Correlation between Na−Cs Ion Exchange Properties in the Alkaline Form and Acid Strength in the Proton Form of Zeolite

Naonobu Katada,* Hayato Tamura, Takuya Matsuda, Yuya Kawatani, Yu Moriwaki, Manami Matsuo, and Ryota Kato

Cite This: *Langmuir* 2024, 40, 19324−19331
Read Online
ACCESS | Metrics & More | Article Recommendations | Supporting Information

**ABSTRACT:** The ion exchange function of zeolite is useful for such a purpose as the removal of radioactive Cs species from water. In the very early days of zeolite science, the affinity of zeolites for metal cations was explained based on geometry. After the explanation presented above was proposed, many new zeolites and related materials were discovered or synthesized. Furthermore, it has become clear that the chemical nature of the ion exchange sites is strongly dependent on the framework topology. In this study, the ion exchange behavior between Na-form zeolites with different framework topologies and Cs-containing aqueous solutions was analyzed, and the equilibrium constant was calculated based on the Langmuir type equation to investigate the influence of the chemical nature of the zeolite framework on ion selectivity. The equilibrium constants at room temperature were in the order **FAU < LTA < MFI < YFI < MOR**. This order is the same as the order of Brønsted acid strengths in the corresponding proton form zeolites. It is suggested that the delocalization of charge around the ion exchange site stabilizes a large cation whose charge is delocalized. In contrast, the equilibrium constant was not related to the pore and cavity size. This opens new insight into the influence of the chemical nature of zeolite on the affinity to cation.

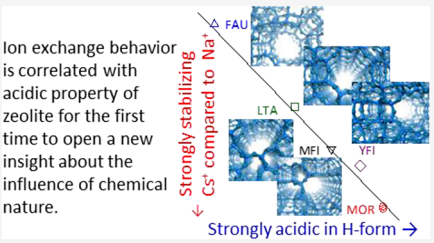


## INTRODUCTION

Separation of $Cs^+$ from aqueous solutions containing $Na^+$ is necessary for the removal of radioactive Cs species in effluents from nuclear facilities[1−36] and for the recovery of Cs as a resource from seawater.[37−40] Na-form zeotypes (zeolites and related materials with zeolitic frameworks) have been utilized in many studies for the separation of $Cs^+$ as ion exchangers or promoters.[5−7,9,10,13,14,17,19,20,22,23,26,29,30,35,36,41,42] Leaching of $Cs^+$ from zeolites has also been investigated for the purpose of immobilizing radioactive Cs species.[41,43−48]

Zeolites are a group of crystalline materials that have a three-dimensional framework consisting of Si−O covalent bonds and micropores resulting from the framework structure, and some of the Si atoms in the framework are replaced with Al atoms. Various types of framework topologies have been discovered and categorized by three-letter framework type codes (FTCs).[49] On the other hand, replacing Si with an oxidation number of +4 with Al with an oxidation number of +3 creates a negative charge that is shared by the Al and the four surrounding O atoms, or the $AlO_4$ unit. In most cases, zeolites are synthesized in basic media containing alkaline cations where one cation is weakly bound to the $AlO_4$ unit. Cations can be exchanged in a variety of media, usually aqueous solutions, and this is the origin of the ion exchange function of zeolite.[50]

The behavior of ion exchange between $Na^+$ and $Cs^+$ on zeolites is classified as Langmuir type,[19,31,51] if it is based on the simplifying assumption that the thermodynamic properties of the ion exchange sites are homogeneous. The ion exchange between Na form zeolite and Cs-containing solution can be depicted as 1

$$Na^+(Z) + Cs^+(aq) \rightarrow Na^+(aq) + Cs^+(Z) \quad (1)$$

where the equilibrium constant $K$ is shown by 2.

$$\frac{\left(\frac{c_{Na^+(aq)}}{c^{\ominus}}\right)\left(\frac{c_{Cs^+(Z)}}{c_{IES(Z)}}\right)}{\left(\frac{c_{Na^+(Z)}}{c_{IES(Z)}}\right)\left(\frac{c_{Cs^+(aq)}}{c^{\ominus}}\right)} = \frac{c_{Na^+(aq)}c_{Cs^+(Z)}}{c_{Na^+(Z)}c_{Cs^+(aq)}} = K \quad (2)$$

where $c_{J(aq)}$ and $c_{J(Z)}$ denote the molarity of chemical species J in the aqueous solution normalized by the volume of the solution and the molarity of species J in the zeolite normalized by the weight of the zeolite, respectively. The symbol $c^{\ominus}$ indicates the molar concentration under standard conditions (1 kmol $m^{-3}$).

Ion exchange capacity $c_{IES(Z)}$ and equilibrium constant $K$ characterize the ion exchange properties of a particular zeolite. The ion exchange capacity $c_{IES(Z)} = c_{Na^+(Z)} + c_{Cs^+(Z)}$, i.e., the

Received: March 5, 2024
Revised: August 4, 2024
Accepted: August 12, 2024
Published: August 21, 2024

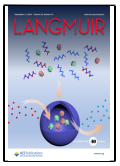





https://doi.org/10.1021/acs.langmuir.4c00801
*Langmuir* 2024, 40, 19324−19331

Table 1. Origin, Chemical Composition of Employed Zeolite Samples and Measured Ion Exchange Parameters

| sample name | origin | framework type | Si/Al molar ratio | $c_{Al(z)}$ (mol kg$^{-1}$) | $c_{IEZ(z)}$ (mol kg$^{-1}$) | $K$ |
|---|---|---|---|---|---|---|
| FAU 6.1 | Na-X type zeolite, Reference Catalyst JRC-Z-NaX2.5(1) supplied by Reference Committee, Catalysis Society of Japan[65] | **FAU** | 1.37 | 6.08 | 0.55 | 3.41 |
| LTA 6.7 | Na-A type zeolite, Zeolum A-4, powder, > 100 mesh, purchased from Tosoh Corp. | **LTA** | 1.12 | 6.69 | 0.18 | 20.4 |
| MFI 1.2 | Na-ZSM-5 type zeolite, International Reference Zeolite IRZ-MFI002 ($NH_4$-MFI, supplied by Catalysis Commission, International Zeolite Association[66]), ion-exchanged with excess of $NaNO_3$. | **MFI** | 12.3 | 1.22 | 1.00 | 50.9 |
| YFI 1.3 | Na-YNU-5 type zeolite, synthesized according to literature,[79] and ion-exchanged with excess of $NaNO_3$. | **YFI** | 11.1 | 1.33 | 0.83 | 73.1 |
| MOR 1.5 | Na-mordenite, HSZ-642NAA supplied by Tosoh Corp. | **MOR** | 9.88 | 1.48 | 1.44 | 177 |
| MOR 1.7 | Na-mordenite, Reference Catalyst JRC-Z-M15(1) supplied by Reference Committee, Catalysis Society of Japan[65] | **MOR** | 8.37 | 1.71 | 1.59 | 187 |

concentration of exchangeable cations per unit weight of the zeolite, depends primarily on the Al content ($c_{Al(Z)}$) but can be influenced by structural properties such as steric hindrance. The equilibrium constant $K$ should reflect the chemical nature of the zeolite.

Affinities to $Na^+$ and $Cs^+$, reflected by the above parameters, are different among zeolites with different compositions and framework topologies. It is known that, among zeolites with a relatively high aluminum concentration, A-type zeolite with **LTA** framework topology has a high $Cs^+$ removal efficiency,[6,8,19] and among zeolites with a moderate Al concentration, mordenite with **MOR** framework topology has a high $Cs^+$ removal efficiency.[17,20] In the very early days of zeolite science, around the 1960s, the affinity of zeolites for metal cations was explained based on geometry, that is, the fitting of the cations to the zeolite cavities.[50,52,53] Differences in the affinity for $Na^+$ and $Cs^+$ between different zeolite species are mainly explained by the sizes of cations and micropores.[23,42,54] In other words, the influences of geometry on the differences in the affinity for $Na^+$ and $Cs^+$, i.e., selectivity in the ion exchange, have been discussed, but the influence of a chemical nature such as acid strength of the zeolite has not been studied.

After the above explanation was proposed, many types of zeotypes with different framework topologies and chemical compositions were discovered or synthesized. Furthermore, over the past three decades, it has become clear that the chemical nature of the ion exchange sites is strongly dependent on the framework topology, as indicated by the striking differences in the Brønsted acid strengths of the H-form.[55,56] It is speculated that the acid strength of H-form zeolite depends on the local geometry, such as the Al−O−Si angle and Al−O distance,[57] and we propose that compression of the Al−OH−Si group from both ends enhances the Brønsted acidity of the proton.[58−60] It is considered necessary to reflect these new findings in the interpretation of the ion exchange properties of the zeolites.

In this study, we analyze the influence of the chemical properties of ion exchange sites on Na−Cs exchange. The equilibrium constant $K$ was analyzed based on the Langmuir model and compared with the Brønsted acid strength of H-form zeolite with the same framework topology.

## EXPERIMENTAL SECTION

The Na-form zeolites shown in Table 1 were used as parent samples. All of them did not contain binders. They are named as shown in Table 1. For example, FAU 6.1 is a zeolite with **FAU** framework topology and 6.1 mol kg$^{-1}$ Al. The structural properties were analyzed as follows: Powder X-ray diffraction (XRD) was recorded using an Ultima IV diffractometer (Rigaku) with a Cu K$\alpha$ X-ray source operated at a voltage of 40 kV and a current of 40 mA, and the reference XRD patterns were obtained from the International Zeolite Association (IZA) Structure Database.[49] The nitrogen adsorption capacity at 77 K was measured using a BEL-Sorp Max (Microtrac BEL) or a BEL-Sorp Mini (Microtrac BEL) after pretreatment at 573 K in a vacuum. The micropore volume and external surface area were estimated from the $t$-plot method.[61] In addition, the micropore volume was estimated also from the amount of liquid nitrogen that filled the micropores when the capillary condensation was completed at $p/p_0$ = 0.005 ($p$ and $p_0$ are the observed pressure and equilibrium vapor pressure at 77 K, respectively, of nitrogen).[62]

Ion exchange between Na form zeolite and Cs-containing solution was examined as follows. An aqueous solution containing 60−360 g m$^{-3}$ of Cs and 1000 g m$^{-3}$ of Na was prepared from ion-exchanged water, cesium nitrate, and sodium nitrate (FUJIFILM Wako Pure Chemicals, Inc.). At room temperature, about 298 K, Na-form zeolite powder (0.1 g) was added to the solution (100 cm$^3$), stirred for 5 min with a magnetic stirrer at about 400 rpm in a conical flask (inner volume 300 cm$^3$), and filtered with a filter paper (No. 101, Advantec, retention particle size 5 $\mu$m). The Cs content of the solution was analyzed by an inductively coupled plasma (ICP) optical emission spectrometer (Agilent 5110). In some cases, the Cs content of the solid was confirmed by ICP analysis after dissolving the solid using hydrofluoric acid.

The analysis was performed from the measured relationship between the Cs content in the zeolite and the solution after ion exchange (Figure S1) as follows. The ion exchange between Na zeolite and a Cs-containing solution can be expressed as 2 where the equilibrium constant is shown by 2. It is assumed that the ion exchange site is covered by $Na^+$ or $Cs^+$. Therefore,

$$c_{Na^+(Z)} + c_{Cs^+(Z)} = c_{IES(Z)}$$

where $c_{IES(Z)}$ denotes the concentration of ion exchange sites responsible for the ion exchange reaction under discussion. Since the substitution of one Si atom (oxidation number +4) by one Al atom (oxidation number +3) in the zeolite framework generates one ion exchange site for charge compensation, the number of ion exchange sites should be equal to $c_{Al(Z)}$, but some ion exchange sites may not be responsible due to steric hindrance or other reasons. Therefore, only functional exchange sites are considered, and in the following analysis, $c_{IES(Z)}$ is used.

From these, 3 is derived.

$$\frac{c_{Cs^+(aq)}}{c_{Cs^+(Z)}} = \frac{1}{c_{IES(Z)}} c_{Cs^+(aq)} + \frac{c_{Na^+(aq)}}{K c_{IES(Z)}} \quad (3)$$

Equation 3 shows that $\frac{c_{Cs^+(aq)}}{c_{Cs^+(Z)}}$ is a linear function of $c_{Cs^+(aq)}$, when measured with varying the $Cs^+$/zeolite ratio and maintaining $c_{Na^+(aq)}$ a constant and high value on one zeolite. Therefore, $c_{IES(Z)}$ and $K$ were determined from the slope and intercept of the plot of $\frac{c_{Cs^+(aq)}}{c_{Cs^+(Z)}}$ against


https://doi.org/10.1021/acs.langmuir.4c00801
Langmuir 2024, 40, 19324−19331

$c_{Cs^+(aq)}$. From $K$, the standard Gibbs energy $\Delta_r G^{\ominus}$ of reaction 1 was calculated by 4.

$$\Delta_r G^{\ominus} = -RT\ln K \quad (4)$$

where $R$ = 8.3145 J K$^{-1}$ mol$^{-1}$ and $T$ was the temperature (298 K).

## RESULTS AND DISCUSSION

**Quality of Parent Zeolite.** XRD measurements of the parent samples showed diffraction patterns consistent with those simulated based on the corresponding crystal types (Figure 1).[49] Nitrogen adsorption on **FAU**, **MFI**, **YFI**, and **MOR** type samples at 77 K showed isotherms classified as type I (Figure 2).[63] The micropore volumes are estimated from the *t*-plot method[61] and also from the micropore condensation capacity.[62] The values estimated by the two methods are similar and are higher than 0.14 cm$^3$ g$^{-1}$ for the parent samples of **FAU**, **MFI**, **YFI**, and **MOR** types (Table 2). These observations demonstrate high crystallinity. In addition, MFI 1.2 is an International Reference Zeolite supplied by IZA (IRZ-MFI002). FAU 6.1 and MOR 1.7 are Reference catalysts from the Catalysis Society of Japan [JRC-Z-NaX2.5 (1) and JRC-Z-M15 (1), respectively]. The physicochemical properties of these samples analyzed by multiple research groups have been opened public.[64−66] On the other hand, LTA 6.7 (Na-A zeolite) showed a quite low nitrogen adsorption capacity at 77 K due to the blocking of the pore opening by Na$^+$ cation.[67−69] This is characteristic of the **LTA-type** zeolite. These results confirm the high crystallinity of the parent zeolites.

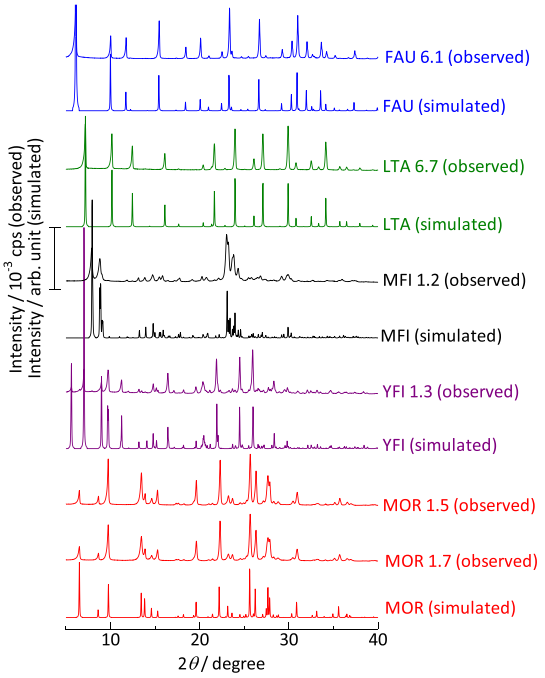


**Figure 1.** X-ray diffraction of parent (Na-form) zeolites. The sample name should be referred to Table 1. Simulated patterns were obtained from the International Zeolite Association (IZA) structure database.[49]

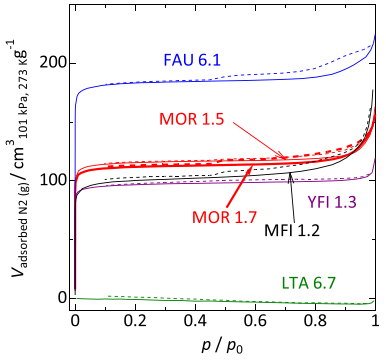


**Figure 2.** Nitrogen adsorption isotherms at 77 K of parent (Na-form) zeolites. Solid and dotted lines show the adsorption and desorption branches, respectively. $p$ and $p_0$ represent the observed pressure and equilibrium vapor pressure at 77 K, respectively, of nitrogen.

**Table 2. Textural Properties Estimated from Nitrogen Adsorption Behavior at 77 K**

| sample name | micropore volume[a] (cm$^3$ g$^{-1}$) | external surface area[b] (m$^2$ g$^{-1}$) |
|---|---|---|
| FAU 6.1 | 0.278 (0.270) | 12.1 |
| LTA 6.7 | not measured[c] | not measured[c] |
| MFI 1.2 | 0.146 (0.148) | 22.3 |
| YFI 1.3 | 0.148 (0.142) | 6.0 |
| MOR 1.5 | 0.175 (0.168) | 8.8 |
| MOR 1.7 | 0.169 (0.163) | 10.5 |

[a]Estimated from *t*-plot method[61] (value from capillary condensation capacity[62] is shown in parentheses). [b]Estimated from the *t*-plot method.[61] [c]Not able to be estimated from nitrogen adsorption due to blocking by Na$^+$.[67−69]

The external surface areas of the **FAU-**, **MFI-**, **YFI-**, and **MOR-type** samples are estimated from the nitrogen adsorption isotherms. In general, the external surface area was small (<23 m$^2$ g$^{-1}$), indicating relatively large crystallite sizes (Table 2).

**Acidic Properties.** Infrared/mass spectroscopy temperature-programmed desorption (IRMS-TPD) of ammonia quantifies the number and strength of each of Brønsted and Lewis acid sites.[70,71] This method has shown that the ammonia desorption enthalpy from the Brønsted acid sites on H-form zeolite, an index of Brønsted acid strength, depends mainly on the type of framework but not on the aluminum concentration.[55,72−75] This is because the Al−O distance mainly controls the acid strength of the Si−OH−Al bridge.[58,60,76] Therefore, it is speculated that an aluminosilicate framework has its own inherent acidity, or electron-withdrawing property, due to its framework topology, and in this study, we compare the Brønsted acid strength of the H-form zeolite and the ion exchange property of the Na-form zeolite.

The ammonia desorption enthalpy from the Brønsted acid sites of H-form zeolite has been found to be 130−140 kJ mol$^{-1}$ for **MFI** with 0.3−1.3 mol kg$^{-1}$ of Al,[55,77] averagely 143 kJ mol$^{-1}$ for **YFI** with 0.3−1.4 mol kg$^{-1}$ of Al[76] and averagely 148 kJ mol$^{-1}$ for **MOR** with 0.4−2.4 mol kg$^{-1}$ of Al.[55,70,72] The Al contents of the parent Na-zeolites (**MFI**: 1.2 mol kg$^{-1}$, **YFI**: 1.3 mol kg$^{-1}$ and **MOR**: 1.5−1.7 mol kg$^{-1}$ as shown in Table 1) were within the above ranges for which the acid strengths of the corresponding H-zeolites have been revealed.

Furthermore, we studied the properties of YFI 1.3 in detail. Although the synthesis lot was different from that in the present study, the composition and synthesis methods were the same. Infrared (IR) spectra of adsorbed $d_3$-acetonitrile, pyridine, and ammonia, the conventional ammonia TPD profile, the TPD profile from Brønsted acid site, and the


https://doi.org/10.1021/acs.langmuir.4c00801
Langmuir 2024, 40, 19324−19331

ammonia desorption enthalpy distribution can be referred to our paper.[76] The applied techniques showed that the Lewis acidity was negligible (0.1 mol $kg^{-1}$), and the number of Brønsted acid sites (1.3 mol $kg^{-1}$) was similar to the number of Al atoms (1.4 mol $kg^{-1}$). These results indicate that most of the Al is incorporated into the framework. The ammonia desorption enthalpy from the Brønsted acid sites was 143 kJ $mol^{-1}$. Therefore, it can be concluded that the Brønsted acid strength of H-form **YFI**, which corresponds to the presently used Na-form sample, is indicated by the ammonia desorption enthalpy of 143 kJ $mol^{-1}$.

MFI 1.2 is an international reference zeolite, and it is opened public[66] that the Brønsted acid amount (1.3 mol $kg^{-1}$) was close to the Al content (1.3 mol $kg^{-1}$), whereas the Lewis acid amount was negligible (0.002 mol $kg^{-1}$), indicating that most of the Al is incorporated into the framework. The ammonia desorption enthalpy of the H-form is reported to be 136 kJ $mol^{-1}$. The conventional ammonia TPD profile, the TPD profile from the Brønsted acid site, and the ammonia desorption enthalpy distribution can be found in public databases, as well as other analytical results.[66]

MOR 1.7 was the subject of group study, and various characterization techniques such as nuclear magnetic resonance (NMR), ammonia TPD, and IR of CO and pyridine showed that most of Al atoms were incorporated into the framework.[64]

The above zeolites (**MFI**, **YFI** and **MOR**) allow comparison of the acidic property of the H-form and the ion exchange property of the Na-form in the same Al concentration range.

On the other hand, in this study, we used Na-form samples of **FAU** and **LTA** with high Al concentrations; **FAU**: 6.1 mol $kg^{-1}$ (X type zeolite), **LTA**: 6.7 mol $kg^{-1}$ (A type zeolite). Zeolites with such high Al concentrations are destroyed in acidic conditions, so conversion into the $NH_4$- or H-form is not possible. However, as mentioned in the previous paragraphs, we speculate that the inherent acidity of the aluminosilicate framework is mainly controlled by the framework topology, allowing us to compare the ion exchange behavior of the Na-form and the acidic property of the H-form even though they have different the aluminum concentrations. The ammonia desorption enthalpy from the Brønsted acid sites was observed to be ca. 110 kJ $mol^{-1}$ for **FAU** (Y type zeolite) with 4.4−5.5 mol $kg^{-1}$ of Al,[72,74,78] and 132 kJ $mol^{-1}$ for **LTA** (UZM-9 type zeolite) with 4.8 mol $kg^{-1}$ of Al,[60] and will be compared with the ion exchange properties in the next section.

**Ion Exchange Properties.** Throughout this study, the ion exchange properties were evaluated by the Cs concentration in the aqueous solution after the ion exchange procedure and the analysis of the Cs contents in the solid was omitted. There are two reasons for this. (1) The final objective of the study is to understand the ion exchange function for the removal of Cs species from water. (2) The dissolution of a small amount of zeolite containing a low concentration of Cs after filtration would result in a large experimental error. However, the analysis of the Cs content was performed on LTA 6.7 under equilibrium with an aqueous solution containing 0.851 mol $m^{-3}$ $Cs^+$ (final composition), followed by dissolution in hydrofluoric acid for ICP analysis. The Cs content in the solid was 0.0579 mol $kg^{-1}$, in agreement with 0.0582 mol $kg^{-1}$ estimated from the solution composition, supporting its validity.

Then, from the analysis of the solutions, the relationship between the compositions of zeolite and solution was estimated in 0−3 mmol $m^{-3}$ region for the zeolite samples used, as shown in Figure S1. From these results, plots of $\frac{c_{Cs^+(aq)}}{c_{Cs^+(Z)}}$ against $c_{Cs^+(aq)}$ are obtained as shown in Figure 3. Nearly

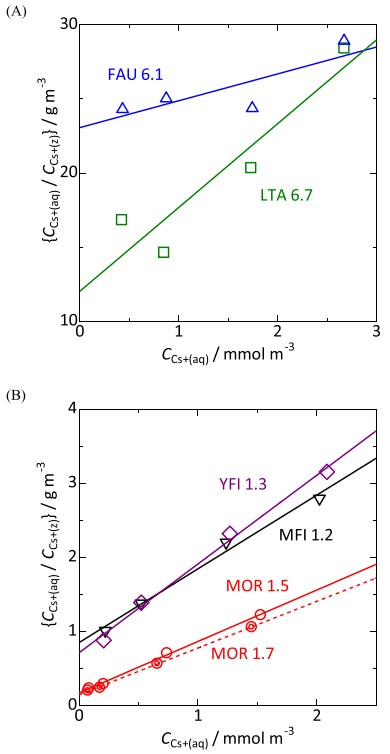


**Figure 3.** Plots of $c_{Cs+(aq)}/c_{Cs+(Z)}$ against $c_{Cs+(aq)}$ on (A) **FAU** and **LTA**, and (B) **MFI**, **YFI** and **MOR** type zeolites.

straight lines were obtained, showing the availability of Langmuir-type analysis using eq 3. From the slope and intercept, the ion exchange capacity $c_{IEZ(Z)}$ and the equilibrium constant $K$ were estimated as shown in Table 1. For reference, the ion-exchange isotherms calculated based on the determined $c_{IEZ(Z)}$ are shown in Figure S2.

For **MFI**-, **YFI**-, and **MOR-type** zeolites, the estimated $c_{IEZ(Z)}$ (the number of sites playing a role of ion exchange sites under the present experimental conditions) was approximately in agreement with $c_{Al(Z)}$ (Figure 4), confirming that one ion exchange site was generated by substitution of one Si (+4) atom by one Al (+3) atom in the framework. However, **FAU** and **LTA** showed far lower $c_{IEZ(Z)}$ values than $c_{Al(Z)}$. Presumably, some of the cations in the sodalite cage, which is separated from the outside by the 6-ring windows, which require high temperature for passage of cations,[50] were not

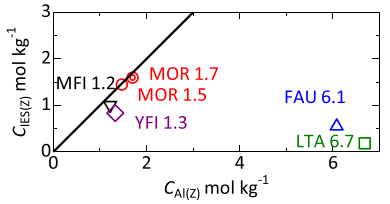


**Figure 4.** Plots of estimated amount of ion exchange sites $c_{IES(Z)}$ against aluminum content $c_{Al(Z)}$. The thick line shows $c_{IES(Z)} = c_{Al(Z)}$.


https://doi.org/10.1021/acs.langmuir.4c00801
Langmuir 2024, 40, 19324−19331

exchanged under these conditions (room temperature). It is noteworthy that wastewater treatment is performed at ambient temperature, and the present experiments demonstrate the ion exchange functions applicable to practical treatment processes.

On the other hand, the calculated $K$ was clearly different among zeolite species as **FAU** < **LTA** < **MFI** < **YFI** < **MOR**, while the difference in $c_{Al(Z)}$ between the two **MOR** samples did not change $K$. The larger $K$ indicates the high ability of Na-form zeolite to remove $Cs^+$ from aqueous solutions in the coexistence of $Na^+$. The high exchange ability of **MOR** is consistent with the preceding literature.[20]

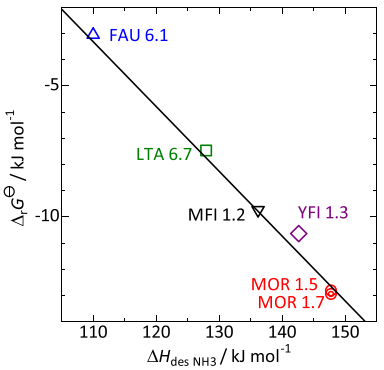


**Figure 5.** Plots of standard Gibbs energy of reaction 1 $\Delta_r G^\ominus$ of zeolites against ammonia desorption enthalpy $\Delta H_{des\ NH3}$ of corresponding H-form zeolites.

As shown in Figure 5, the standard Gibbs energy $\Delta_r G^\ominus$ of the ion exchange (1) decreases with the increase in ammonia desorption enthalpy from the Brønsted acid sites of the corresponding H-form zeolite. Since ammonia desorption enthalpy (heat of ammonia adsorption) is an indicator of acid strength, this indicates that the zeolite framework, which generates strong Brønsted acidity in the H-form, strongly stabilizes $Cs^+$.

As mentioned above, we propose that the Brønsted acid strength of the Si−OH−Al bridge is controlled by the Al−O distance, suggesting that the acid strength (electron withdrawing property) is due to structural stress. An H-form zeolite has $Al(-O-Si)_4$ units where $H^+$ is bonded to one of the four O atoms. Theoretical calculations reveal that the O−H bond is a covalent bond, not an ionic bond, and the Al−O distance in Al−OH−Si becomes longer than the other three Al−O distances. In the $NH_4$ form, the $NH_4^+$ cation does not have a covalent bond with the framework atoms and is usually coordinated to two oxygen atoms. The four Al−O distances are similar and shorter than the Al−O distance in the Al−OH−Si of the H-form.[58] Meanwhile, there are complex mechanical forces around the Al−O−Si bridge. Theoretical calculations reveal that the stress and compression from both ends of Al−O−Si change the distance between Al−O, and the shorter the Al−O, the higher the desorption energy (enthalpy) of ammonia.[58]

In the case of Al−O−Si compressed from both ends, the geometry in which the distance between all four Al−Os is the same is relatively stable (Scheme 1A), whereas in the case of Al−O−Si stretched from both ends, the geometry in which one Al−O distance is longer is relatively stable (B). In the former, the negative charge generated by the isomorphous substitution of $Si^{4+}$ by $Al^{3+}$ is delocalized, and the charge is shared by four oxygen atoms. In contrast, in the latter, the negative charge is localized on one oxygen atom. A cation with a positive charge delocalized over a wide space, i.e., a soft Lewis acid, prefers the former Al−O−Si (soft Lewis base), while a hard Lewis acid prefers the latter hard Lewis base.

$NH_4^+$ is a larger and therefore softer Lewis acid than $H^+$. The strong Brønsted acidity means instability of $H^+$, and more exactly, high ammonia desorption energy means the stability of $NH_4^+$ compared to $H^+$ on the discussed ion exchange site. It reflects the softness of the Lewis base property of the site.

On the other hand, $Cs^+$ is larger and therefore softer Lewis acid than $Na^+$. $Cs^+$ should prefer a soft Lewis base, i.e., the $Al(-O-Si)_4$ group with equal Al−O distances and a shared negative charge on four oxygen atoms. This tendency should be common for the cases of ammonia adsorption ($H^+ \rightarrow NH_4^+$) and Na−Cs exchange ($Na^+ \rightarrow Cs^+$). Thus, the influence of the chemistry of the silicate framework on the selectivity of ions can be explained.

**Scheme 1. Schematic Drawings of Influence of Local Geometry on Charge Localization around Ion Exchange Sites**[a]

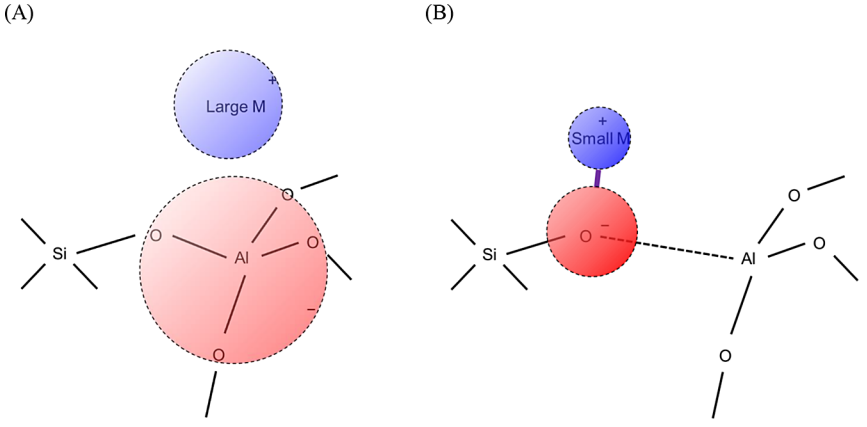


[a](A) shows a Si−O−Al bridge compressed from both ends, whose negative charge is delocalized, strongly acidic (prefers $NH_4^+$ than $H^+$), and prefers $Cs^+$ than $Na^+$. (B) shows a Si−O−Al bridge stretched from both ends, whose negative charge is localized to an O atom, weakly acidic (prefers $H^+$ than $NH_4^+$), and prefers $Na^+$ than $Cs^+$.



https://doi.org/10.1021/acs.langmuir.4c00801
Langmuir 2024, 40, 19324−19331

In contrast, the equilibrium constant $K$ or the Gibbs energy $\Delta_r G^{\ominus}$ was not related to the pore and cavity size of these zeolites (representative parameters are shown in Table S1). At least for the four framework types treated in this study, it can be said that chemical properties have a stronger influence than porosity.

## CONCLUSIONS

The analysis of ion exchange behavior between Na-type zeolite and Cs-containing aqueous solution showed that the equilibrium constants at room temperature were in the order **FAU** < **LTA** < **MFI** < **YFI** < **MOR**, as the order of Brønsted acid strengths in the corresponding proton form zeolites. The Gibbs energy of ion exchange, which reflects the above equilibrium constant, showed a linear relationship with the ammonia desorption enthalpy from the Brønsted acid sites on the proton form zeolites, an indicator of the Brønsted acid strength. In contrast, the equilibrium constant was not related to the pore and cavity size. At least for the four framework types treated in the present study, it can be said that chemical properties have a stronger influence than porosity.

## ASSOCIATED CONTENT

### Supporting Information

The Supporting Information is available free of charge at https://pubs.acs.org/doi/10.1021/acs.langmuir.4c00801.

Microporous properties of frameworks, compositions of solvent and zeolite after the ion exchange, and ion exchange isotherms (PDF)

## AUTHOR INFORMATION


### Corresponding Author

**Naonobu Katada** − *Center for Research on Green Sustainable Chemistry, Faculty of Engineering, Tottori University, Tottori 680-8552, Japan*; orcid.org/0000-0002-2288-595X; Email: katada@tottori-u.ac.jp

### Authors

**Hayato Tamura** − *Tottori University Junior High School, Tottori 680-0945, Japan*

**Takuya Matsuda** − *Center for Research on Green Sustainable Chemistry, Faculty of Engineering, Tottori University, Tottori 680-8552, Japan*

**Yuya Kawatani** − *Center for Research on Green Sustainable Chemistry, Faculty of Engineering, Tottori University, Tottori 680-8552, Japan*

**Yu Moriwaki** − *Center for Research on Green Sustainable Chemistry, Faculty of Engineering, Tottori University, Tottori 680-8552, Japan*

**Manami Matsuo** − *Center for Research on Green Sustainable Chemistry, Faculty of Engineering, Tottori University, Tottori 680-8552, Japan*

**Ryota Kato** − *Center for Research on Green Sustainable Chemistry, Faculty of Engineering, Tottori University, Tottori 680-8552, Japan*

Complete contact information is available at: https://pubs.acs.org/10.1021/acs.langmuir.4c00801


### Notes

The authors declare no competing financial interest.

## ACKNOWLEDGMENTS

This research was carried out as part of the Tottori University Junior Doctor Training School, Environmental Research Program with support from the JST Next Generation Human Resources Development Project. We also received support from JSPS KAKENHI (21H01717, 23H05454).

## REFERENCES


(1) Andreeva, N. R.; Shubaeva, M. A. Ion-exchange properties of geolite k-g relative to strontium and cesium. *Sov. Radiochem.* **1989**, *31* (4), 469−473.

(2) Solache-Rios, M.; Garcia-Sosa, I.; Sosa-Reyes, S. Ethylenediamine effect on the sorption of cesium on zeolites ZSM-5 and Y. *J. Radioanal. Nucl. Chem.* **1998**, *237* (1−2), 151−153.

(3) Sylvester, P.; Clearfield, A.; Diaz, R. J. Pillared montmorillonites: Cesium-selective ion-exchange materials. *Sep. Sci. Technol.* **1999**, *34* (12), 2293−2305.

(4) Qian, G. R.; Li, Y. X.; Yi, F. C.; Shi, R. M. Improvement of metakaolin on radioactive Sr and Cs immobilization of alkali-activated slag matrix. *J. Hazard. Mater.* **2002**, *92* (3), 289−300.

(5) Goni, S.; Guerrero, A.; Lorenzo, M. P. Efficiency of fly ash belite cement and zeolite matrices for immobilizing cesium. *J. Hazard. Mater.* **2006**, *137* (3), 1608−1617.

(6) El-Naggar, M. R.; El-Kamash, A. M.; El-Dessouky, M. I.; Ghonaim, A. K. Two-step method for preparation of NaA-X zeolite blend from fly ash for removal of cesium ions. *J. Hazard. Mater.* **2008**, *154* (1−3), 963−972.

(7) Rajec, P.; Domianovia, K. Cesium exchange reaction on natural and modified clinoptilolite zeolites. *J. Radioanal. Nucl. Chem.* **2008**, *275* (3), 503−508.

(8) Iucolano, F.; Liguori, B.; Sabova, L.; Chmielewska, E.; Caputo, D.; Colella, C. Safe trapping of Cs in heat-treated zeolite matrices. In *Part 2, 4th Conference of the Federation of European Zeolite Associations (FEZA), Univ Pierra Marie Curie, Paris, France, Sep 02−06*; Univ Pierra Marie Curie: Paris, France, 2008; pp 537−540.

(9) El-Kamash, A. M. Evaluation of zeolite A for the sorptive removal of Cs+ and Sr2+ ions from aqueous solutions using batch and fixed bed column operations. *J. Hazard. Mater.* **2008**, *151* (2−3), 432−445.

(10) Borai, E. H.; Harjula, R.; Malinen, L.; Paajanen, A. Efficient removal of cesium from low-level radioactive liquid waste using natural and impregnated zeolite minerals. *J. Hazard. Mater.* **2009**, *172* (1), 416−422.

(11) Bayulken, S.; Bascetin, E.; Guclu, K.; Apak, R. Investigation and Modeling of Cesium(I) Adsorption by Turkish Clays: Bentonite, Zeolite, Sepiolite, and Kaolinite. *Environ. Prog. Sustain. Energy* **2011**, *30* (1), 70−80.

(12) Sekizawa, H.; Yamashita, S.; Tanji, K.; Okoshi, S.; Yoshioka, K. Reduction of Radioactive Cesium in Apple Juice by Zeolite. *Nippon Shokuhin Kagaku Kogaku Kaishi* **2013**, *60* (5), 212−217.

(13) Johan, E.; Yamada, T.; Munthali, M. W.; Kabwadza-Corner, P.; Aono, H.; Matsue, N. Natural zeolites as potential materials for decontamination of radioactive cesium. In *5th Sustainable Future for Human Security (SustaiN), Bali, Indonesia, Oct 19−21*; Bali, Indonesia, 2014; pp 52−56.

(14) Torad, N. L.; Naito, M.; Tatami, J.; Endo, A.; Leo, S. Y.; Ishihara, S.; Wu, K. C. W.; Wakihara, T.; Yamauchi, Y. Highly Crystallized Nanometer-Sized Zeolite A with Large Cs Adsorption Capability for the Decontamination of Water. *Chem. − Asian J.* **2014**, *9* (3), 759−763.

(15) Lihareva, N.; Kostov-Kytin, V. Sorption of Cs+ by nano-sized microporous titanium silicates with pharmacosiderite structure. *Bulg. Chem. Commun.* **2014**, *46* (3), 569−575.

(16) Sano, M.; Nakagawa, K.; Oda, H.; Obata, H.; Kitani, S.; Yamazaki, K. Fundamental Study for the Development of Cs Removal Technique from Low Level Radioactive Liquid Wastes of Decontamination Processes. *Kagaku Kogaku Ronbun* **2014**, *40* (3), 261−265.

(17) Yamada, K.; Johan, E.; Matsue, N.; Itagaki, Y.; Aono, H. Preparation of mordenite and its composite material with nano-sized magnetite from diatomites for radioactive Cs decontamination. *J. Ceram. Soc. Jpn.* **2015**, *123* (1435), 129−135.
(18) Ozeki, K.; Aoki, H. Evaluation of the adsorptive behavior of cesium and strontium on hydroxyapatite and zeolite for decontamination of radioactive substances. *Biomed. Mater. Eng.* **2016**, *27* (2−3), 227−236.
(19) Vipin, A. K.; Ling, S.; Fugetsu, B. Removal of Cs+ and Sr2+ from water using MWCNT reinforced Zeolite-A beads. *Microporous Mesoporous Mater.* **2016**, *224*, 84−88.
(20) Aono, H.; Kaji, N.; Itagaki, Y.; Johan, E.; Matsue, N. Synthesis of mordenite and its composite material using chemical reagents for Cs decontamination. *J. Ceram. Soc. Jpn.* **2016**, *124* (5), 617−623.
(21) Ishikawa, N. K.; Kuwata, M.; Ito, A.; Umita, T. Effect of pH and Chemical Composition of Solution on Sorption and Retention of Cesium by Feldspar, Illite, and Zeolite as Cesium Sorbent From Landfill Leachate. *Soil Sci.* **2017**, *182* (2), 63−68.
(22) Palamarchuk, M.; Egorin, A.; Tokar, E.; Tutov, M.; Marinin, D.; Avramenko, V. Decontamination of spent ion-exchangers contaminated with cesium radionuclides using resorcinol-formaldehyde resins. *J. Hazard. Mater.* **2017**, *321*, 326−334.
(23) Lee, H. Y.; Kim, H. S.; Jeong, H.-K.; Park, M.; Chung, D.-Y.; Lee, K.-Y.; Lee, E.-H.; Lim, W. T. Selective Removal of Radioactive Cesium from Nuclear Waste by Zeolites: On the Origin of Cesium Selectivity Revealed by Systematic Crystallographic Studies. *J. Phys. Chem. C* **2017**, *121* (19), 10594−10608.
(24) Wu, Y.; Zhang, X. X.; Wei, Y. Z.; Mimura, H. Development of adsorption and solidification process for decontamination of Cs-contaminated radioactive water in Fukushima through silica-based AMP hybrid adsorbent. *Sep. Purif. Technol.* **2017**, *181*, 76−84.
(25) Kim, G. N.; Kim, S. S.; Choi, J. W. Development of an agent suited for adsorbing Cs-137 from ash and soil waste solutions. *Sep. Purif. Technol.* **2017**, *173*, 193−199.
(26) Sterba, J. H.; Sperrer, H.; Wallenko, F.; Welch, J. M. Adsorption characteristics of a clinoptilolite-rich zeolite compound for Sr and Cs. *J. Radioanal. Nucl. Chem.* **2018**, *318* (1), 267−270.
(27) Belousov, P.; Semenkova, A.; Egorova, T.; Romanchuk, A.; Zakusin, S.; Dorzhieva, O.; Tyupina, E.; Izosimova, Y.; Tolpeshta, I.; Chernov, M.; Krupskaya, V. Cesium Sorption and Desorption on Glauconite, Bentonite, Zeolite, and Diatomite. *Minerals* **2019**, *9* (10), 625.
(28) Eljamal, O.; Shubair, T.; Tahara, A.; Sugihara, Y.; Matsunaga, N. Iron based nanoparticles-zeolite composites for the removal of cesium from aqueous solutions. *J. Mol. Liq.* **2019**, *277*, 613−623.
(29) Ding, D.; Li, K. X.; Fang, D. Z.; Ye, X. S.; Hu, Y. Q.; Tan, X. L.; Liu, H. N.; Wu, Z. J. Novel Biomass-Derived Adsorbents Grafted Sodium Titanium Silicate with High Adsorption Capacity for Rb+ and Cs+ in the Brine. *Chemistryselect* **2019**, *4* (46), 13630−13637.
(30) Tuaimah, S. K.; Al-Nasri, S. K.; Al-Rahmani, A. A.; Abbas, T. K. Using Dates Leaves Midribs to Prepare Hierarchical Structures Incorporating Porous Carbon and Zeolite A Composites for Cesium Cs-137 Ion Exchange. *Baghdad Sci. J.* **2020**, *17* (3), 818−825.
(31) Liao, H. Y.; Li, Y.; Li, H. R.; Li, B. L.; Zhou, Y. Z.; Liu, D. B.; Wang, X. L. Efficiency and mechanism of amidoxime-modified X-type zeolite (AO-XZ) for Cs+ adsorption. *Chem. Phys. Lett.* **2020**, *741*, No. 137084.
(32) Lee, Y.; Park, C. W.; Kim, H. J.; Kim, S. J.; Lee, T. S.; Yang, H. M. Sulfur-encapsulated zeolite micromotors for the selective removal of cesium from high-salt water with accelerated cleanup times. *Chemosphere* **2021**, *276*, No. 130190.
(33) Yanaka, A.; Shibata, K.; Matsumoto, N.; Yoshida, H. STUDY ON REMOVAL OF CESIUM FROM CONTAMINATED SOIL BY ELECTROPHORESIS USING POTASSIUM ACETATE AS ELECTROLYTE. *Int. J. Geomate* **2021**, *20* (81), 16−21.
(34) Ferreira, D. R.; Phillips, G. D.; Baruah, B. A COMPARISON OF THE ADSORPTION OF CESIUM ON ZEOLITE MINERALS VS VERMICULITE. *Clays Clay Miner.* **2021**, *69* (6), 663−671.
(35) Abbas, T. K.; Rashid, K. T.; Alsalhy, Q. F. NaY zeolite-polyethersulfone-modified membranes for the removal of cesium-137 from liquid radioactive waste. *Chem. Eng. Res. Des.* **2022**, *179*, 535−548.
(36) Arbel-Haddad, M.; Harnik, Y.; Schlosser, Y.; Goldbourt, A. Cesium immobilization in metakaolin-based geopolymers elucidated by Cs-133 solid state NMR spectroscopy. *J. Nucl. Mater.* **2022**, *562*, No. 153570.
(37) Zhang, N.; Gao, D. L.; Liu, M. M.; Deng, T. L. Rubidium and Cesium Recovery from Brine Resources. *Adv. Mater. Res.* **2014**, *1015*, 417−420.
(38) Ali, A.; Quist-Jensen, C. A., Chapter 18 - Membrane Operations for Minerals' Recovery From Seawater. In *Current Trends and Future Developments on (Bio-) Membranes*; Basile, A.; Curcio, E.; Inamuddin, Eds.; Elsevier: 2019; pp 449−471.
(39) Zhang, X.; Zhao, W.; Zhang, Y.; Jegatheesan, V. A review of resource recovery from seawater desalination brine. *Rev. Environ. Sci. Biotechnol.* **2021**, *20* (2), 333−361.
(40) Chen, S.; Dong, Y.; Wang, H.; Sun, J.; Wang, J.; Zhang, S.; Dong, H. Highly efficient and selective cesium recovery from natural brine resources using mesoporous Prussian blue analogs synthesized by ionic liquid-assisted strategy. *Resour. Conserv. Recycl.* **2022**, *186*, No. 106542.
(41) Belkhiri, S.; Guerza, M.; Chouikh, S.; Boucheffa, Y.; Mekhalif, Z.; Delhalle, J.; Colella, C. Textural and structural effects of heat treatment and γ-irradiation on Cs-exchanged NaX zeolite, bentonite and their mixtures. *Microporous Mesoporous Mater.* **2012**, *161*, 115−122.
(42) Malek, A.; Ozin, G. A.; Macdonald, P. M. Probing cation sites in cesium-exchanged zeolite Y via Cs-133 MAS NMR. *J. Phys. Chem.* **1996**, *100* (41), 16662−16666.
(43) Lima, E. J.; Ibarra, I. A.; Vera, M. A.; Lara, V. H.; Bosch, P.; Bulbulian, S. I. Cesium leaching in CsA and CsX zeolites. *J. Phys. Chem. B* **2004**, *108* (32), 12103−12110.
(44) Ibarra, I. A.; Lima, E.; Loera, S.; Bosch, P.; Bulbulian, S.; Lara, V. II. Cesium leaching in CsA and CsX zeolites: Use of blocking agents to inhibit the cesium cation mobility. *J. Phys. Chem. B* **2006**, *110* (42), 21086−21091.
(45) Lima, E.; Ibarra, I. A.; Lara, V.; Bosch, P.; Bulbulian, S. Cesium leaching from gamma-irradiated CsA and CsX zeolites. *J. Hazard. Mater.* **2008**, *160* (2−3), 614−620.
(46) Tansho, M.; Tamura, K.; Shimizu, T. Identification of Multiple Cs+ Adsorption Sites in a Hydroxy-interlayered Vermiculite-like Layered Silicate through Cs-133 MAS NMR Analysis. *Chem. Lett.* **2016**, *45* (12), 1385−1387.
(47) Yabiki, K.; Eba, H.; Sakurai, K. Behavior and Mechanism of Cesium Adsorption on Layered Sodium Silicate Ilerite. *Kagaku Kogaku Ronbun* **2016**, *42* (1), 1−7.
(48) Kuroda, K.; Toda, K.; Kobayashi, Y.; Sato, T.; Otake, T. Cs Leaching Behavior During Alteration Process of Calcium Silicate Hydrate and Potassium Alumino Silicate Hydrate. In *14th International Congress for Applied Mineralogy (ICAM), Belgorod, RUSSIA-Belgorod, Russia, Belgorod Technol UnivBelgorod Technol Univ: Sep 23−27*; Belgorod Technol Univ: Belgorod, Russia, 2019; pp 451−452.
(49) Baerlocher, C.; McCusker, L. B. Database of Zeolite Structures. http://www.iza-structure.org/databases/ (accessed 2023/12/11).
(50) Breck, D. W., Ion Exchange Reactions in Zeolites. In *Zeolite Molecular Sieves: Structure, Chemistry, and Use*; Wiley: 1974; pp 529−592.
(51) Lihareva, N.; Petrov, O.; Tzvetanova, Y. Modelling of Cs+ uptake by natural clinoptilolite from water media. *Bulg. Chem. Commun.* **2017**, *49* (3), 577−582.
(52) Sherry, H. S.; Walton, H. F. The ion-exchange properties of zeolites. II. Ion exchange in the synthetic zeolite Linde 4A. *J. Phys. Chem.* **1967**, *71* (5), 1457−1465.
(53) Sherry, H. S. The Ion-Exchange Properties of Zeolites. I. Univalent Ion Exchange in Synthetic Faujasite. *J. Phys. Chem.* **1966**, *70* (4), 1158−1168.


https://doi.org/10.1021/acs.langmuir.4c00801
*Langmuir* 2024, 40, 19324−19331

(54) Liu, H. M.; Grey, C. P. Probing Cs+ cation accessibility with O-2 and Cs-133 MAS NMR spectroscopy. *Microporous Mesoporous Mater.* **2002**, *53* (1−3), 109−120.
(55) Katada, N.; Igi, H.; Kim, J. H.; Niwa, M. Determination of the acidic properties of zeolite by theoretical analysis of temperature-programmed desorption of ammonia based on adsorption equilibrium. *J. Phys. Chem. B* **1997**, *101* (31), 5969−5977.
(56) Niwa, M.; Katada, N.; Okumura, K. Solid Acidity of Zeolites. *In Springer Ser. Mater. S* **2010**, *141*, 9−27.
(57) Senchenya, I. N.; Kazansky, V. B.; Beran, S. Quantum Chemical Study of the Effect of the Structural Characteristics of Zeolites on the Properties of Their Bridging Oh Groups. Part 2. *J. Phys. Chem.* **1986**, *90* (20), 4857−4859.
(58) Katada, N.; Suzuki, K.; Noda, T.; Sastre, G.; Niwa, M. Correlation between Bronsted Acid Strength and Local Structure in Zeolites. *J. Phys. Chem. C* **2009**, *113* (44), 19208−19217.
(59) Suzuki, K.; Katada, N.; Niwa, M. Measurements of Acidity of H-SSZ-35 by a Combined Method of IRMS-TPD Experiment and DFT Calculation. *Catal. Lett.* **2010**, *140* (3−4), 134−139.
(60) Katada, N.; Nouno, K.; Lee, J. K.; Shin, J.; Hong, S. B.; Niwa, M. Acidic Properties of Cage-Based, Small-Pore Zeolites with Different Framework Topologies and Their Silicoaluminophosphate Analogues. *J. Phys. Chem. C* **2011**, *115* (45), 22505−22513.
(61) Voogd, P.; Scholten, J. J. F.; van Bekkum, H. Use of the t-plot—De Boer method in pore volume determinations of ZSM-5 type zeolites. *Colloids Surf.* **1991**, *55*, 163−171.
(62) Nakajima, K.; Suganuma, S.; Tsuji, E.; Katada, N. Mechanism of tetralin conversion on zeolites for the production of benzene derivatives. *React. Chem. Eng.* **2020**, *5* (7), 1272−1280.
(63) Sing, K. S. W. Reporting physisorption data for gas/solid systems with special reference to the determination of surface area and porosity (Recommendations 1984). *Pure Appl. Chem.* **1985**, *57* (4), 603−619.
(64) Katada, N.; Takeguchi, T.; Suzuki, T.; Fukushima, T.; Inagaki, K.; Tokunaga, S.; Shimada, H.; Sato, K.; Oumi, Y.; Sano, T.; Segawa, K.; Nakai, K.; Shoji, H.; Wu, P.; Tatsumi, T.; Komatsu, T.; Masuda, T.; Domen, K.; Yoda, E.; Kondo, J. N.; Okuhara, T.; Kageyama, Y.; Niwa, M.; Ogura, M.; Matsukata, M.; Kikuchi, E.; Okazaki, N.; Takahashi, M.; Tada, A.; Tawada, S.; Kubota, Y.; Sugi, Y.; Higashio, Y.; Kamada, M.; Kioka, Y.; Yamamoto, K.; Shouji, T.; Arima, Y.; Okamoto, Y.; Matsumoto, H. Standardization of catalyst preparation using reference catalyst: ion exchange of mordenite type zeolite - 1. Remarkable dealumination accompanying ion exchange. *Appl. Catal., A* **2005**, *283* (1−2), 63−74.
(65) Reference Catalyst Committee. Catalysis Society of Japan, Reference Catalyst Portal. https://jrc.catsj.jp/JRCpublic.html (accessed 2023/12/11).
(66) Catalysis Commission, International Zeolite Association, International Reference Zeolite. http://www.iza-online.org/catalysis/referencezeolite.htm (accessed 2023/12/11).
(67) Sebastian, J.; Pillai, R. S.; Peter, S. A.; Jasra, R. V. Sorption of N2, O2, and Ar in Mn(II)-Exchanged Zeolites A and X Using Volumetric Measurements and Grand Canonical Monte Carlo Simulation. *Ind. Eng. Chem. Res.* **2007**, *46* (19), 6293−6302.
(68) Shang, Y.; Wu, J.; Zhu, J.; Wang, Y.; Meng, C. Study on adsorption of N2 and O2 by magnesium (II)-exchanged zeolite A. *J. Alloys Compd.* **2009**, *478* (1), L5−L7.
(69) Palomino, M.; Corma, A.; Rey, F.; Valencia, S. New Insights on CO2−Methane Separation Using LTA Zeolites with Different Si/Al Ratios and a First Comparison with MOFs. *Langmuir* **2010**, *26* (3), 1910−1917.
(70) Niwa, M.; Suzuki, K.; Katada, N.; Kanougi, T.; Atoguchi, T. Ammonia IRMS-TPD study on the distribution of acid sites in mordenite. *J. Phys. Chem. B* **2005**, *109* (40), 18749−18757.
(71) Niwa, M.; Katada, N. New Method for the Temperature-Programmed Desorption (TPD) of Ammonia Experiment for Characterization of Zeolite Acidity: A Review. *Chem. Rec.* **2013**, *13* (5), 432−455.
(72) Katada, N.; Kageyama, Y.; Niwa, M. Acidic property of Y- and mordenite-type zeolites with high aluminum concentration under dry conditions. *J. Phys. Chem. B* **2000**, *104* (31), 7561−7564.
(73) Miyamoto, Y.; Katada, N.; Niwa, M. Acidity of beta zeolite with different Si/Al-2 ratio as measured by temperature programmed desorption of ammonia. *Microporous Mesoporous Mater.* **2000**, *40* (1−3), 271−281.
(74) Katada, N.; Kageyama, Y.; Takahara, K.; Kanai, T.; Begum, H. A.; Niwa, M. Acidic property of modified ultra stable Y zeolite: increase in catalytic activity for alkane cracking by treatment with ethylenediaminetetraacetic acid salt. *J. Mol. Catal. A: Chem.* **2004**, *211* (1−2), 119−130.
(75) Katada, N.; Niwa, M. Analysis of acidic properties of zeolitic and non-zeolitic solid acid catalysts using temperature-programmed desorption of ammonia. *Catal. Surv. Asia* **2004**, *8* (3), 161−170.
(76) Katada, N.; Yamamoto, K.; Fukui, M.; Asanuma, K.; Inagaki, S.; Nakajima, K.; Suganuma, S.; Tsuji, E.; Palcic, A.; Valtchev, V.; Petkov, P. S.; Simeonova, K.; Vayssilov, G. N.; Kubota, Y. Acidic property of YNU-5 zeolite influenced by its unique micropore system. *Microporous Mesoporous Mater.* **2022**, *330*, No. 111592.
(77) Suganuma, S.; Nakamura, K.; Okuda, A.; Katada, N. Enhancement of catalytic activity for toluene disproportionation by loading Lewis acidic nickel species on ZSM-5 zeolite. *Mol. Catal.* **2017**, *435*, 110−117.
(78) Suzuki, K.; Katada, N.; Niwa, M. Detection and quantitative measurements of four kinds of OH in HY zeolite. *J. Phys. Chem. C* **2007**, *111* (2), 894−900.
(79) Nakazawa, N.; Ikeda, T.; Hiyoshi, N.; Yoshida, Y.; Han, Q.; Inagaki, S.; Kubota, Y. A Microporous Aluminosilicate with 12-, 12-, and 8-Ring Pores and Isolated 8-Ring Channels. *J. Am. Chem. Soc.* **2017**, *139* (23), 7989−7997.


https://doi.org/10.1021/acs.langmuir.4c00801
*Langmuir* 2024, 40, 19324−19331